Intra-thalamic and Thalamocortical Connectivity: Potential Implication for Deep Learning

Jie Mei
Charité – Universitätsmedizin Berlin
Berlin, Germany
jie.mei@deepkapha.ai

Tarry Singh
deepkapha.ai
Amsterdam, Netherlands
tarry.singh@deepkapha.ai

ABSTRACT

Contrary to the traditional view that the thalamus acts as a passive relay station of sensory information to the cortex, a number of experimental studies have demonstrated the effects of peri-geniculate and cortico-thalamic projections on the transmission of visual input. In the present study, we implemented a mechanistic model to facilitate the understanding of peri-geniculate and cortico-thalamic effects on the transfer function of geniculate cells and their firing patterns. As a result, the model successfully captures some fundamental properties of early-stage visual processing in mammalian brain. We conclude, therefore, that the thalamus is not a passive relay center and the intra-thalamic circuitry is of great importance to biological vision. In summary, intra-thalamic and thalamocortical circuitries have implications in early-stage visual processing, and could constitute a valid tool for refining information relay and compression in artificial neural networks (ANN), leading to deep learning models of higher performance.

KEYWORDS

thalamus, thalamocortical circuitry, computational model, biological vision, deep learning

1 INTRODUCTION

For decades, neuroscientists have considered the thalamus as a passive relay center for transmission of sensory information to the cortex. However, more recent evidence has challenged this traditional view [19, 28]. Lateral geniculate nucleus (LGN), the visual part of the dorsal thalamus, receives intensive feedback innervation from both the peri-geniculate nucleus (PGN) and the visual cortex while sending visual information to the cortex. With the aim of investigating the functional properties of the LGN–PGN loop, we constructed biologically-detailed models using the NEURON simulator [12], which were able to produce simulation results that are consistent with experimental data.

SE4COG'18, May 28–29, 2018, Gothenburg, Sweden

ACM ISBN 978-1-4503-5740-1/18/05…$15.00
https://doi.org/10.1145/3195555.3195556

1.1 The Thalamus

The thalamus is responsible for sensory and motor signal transmission to the cerebral cortex as well as the regulation of sleep, wakefulness and alertness [26]. Dorsal thalamus is the largest part of the diencephalon, through which all sensory information, except olfactory, passes on its way to cortex. LGN is the nucleus responsible for visual processing in the dorsal thalamus. Ventral thalamus does not send any axons to the cortex. The major part of the ventral thalamus is the thalamic reticular nucleus (TRN), which envelops the dorsal thalamus.

1.2 Thalamic Triad, LGN–PGN Loop and Thalamocortical Connectivity

1.2.1 Thalamic Triad. A thalamic triad is a complex synaptic arrangement in the thalamus which involves three synapses. In LGN, the axonal terminal of retinal ganglion cell enters thalamic triad, contacts both principal relay cell and neighboring interneuron (two major types of neurons in LGN) and sends information to both (Figure 1).

1.2.2 LGN–PGN Loop. The PGN has been regarded as a key player in several physiological functions, including gain control of retino-geniculate transmission [27]. Principal relay cells send excitatory afferents to PGN and receive inhibitory projections from PGN reticular cells. *In vivo* and *in vitro* studies have shown that LGN–PGN connectivity produces oscillatory firing, such as sleep-spindles, which primarily occur during sleep onset and drowsiness [29].

1.2.3 Feedback Connections from the Cortex. While sending axons to the visual cortex, LGN receives projections from cortical layer 6 cells. Extensive innervation from the visual cortex accounts for approximately 30% of input to LGN relay cells, while retinal afferents comprise only 10% [28]. Thus, in contrast to previously thought, the thalamus yields complicated intrinsic properties which may contribute to information processing and transmission.

2 MODELING THE LGN–PGN CONNECTIVITY

In this study, multi-compartmental models incorporating LGN principal relay cells, interneurons and PGN reticular cells were implemented using the NEURON platform [12]. Cell morphologies of all cells were adapted from previous studies [3, 4, 10]. Parameters in the model were adapted from experimental literature as much as possible to ensure biological plausibility. Results obtained from computational simulations were validated with respect to experimental data [7, 16, 24].

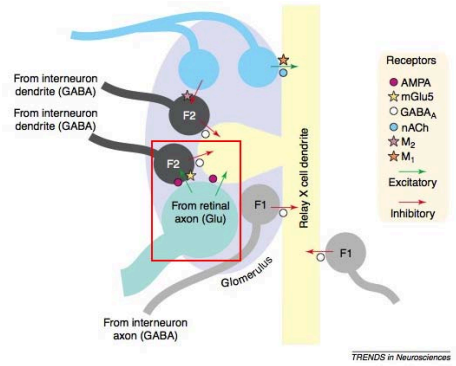

Figure 1: **Schematic diagram of a thalamic triad. Red rectangle: three synapses of the thalamic triad; pale green: retinal ganglion cell axon; black: LGN interneuron dendritic terminal (F2, F stands for 'flattened vesicle'); gray: LGN interneuron axonal terminal (F1); yellow: LGN principal relay cell dendrite; blue: parabrachial terminal from brainstem. From [25].**

2.1 Methods

Neurons in the LGN and PGN were built as multi-compartmental, Hodgkin-Huxley-type kinetic models [14]. Three network topologies were studied. Version 7.3 of NEURON simulation environment with the Python interface [13] was used in all simulations.

2.2 Implementing the Cells

2.2.1 Retinal Input. Virtual Retina, a large scale simulator of the biological retina [31], was used to generate artificial spike trains from .gif images for modeling visual inputs.

2.2.2 LGN and PGN Cells. LGN principal relay cells, interneurons and PGN reticular cells were modeled with biologically-detailed 3-D morphologies. All model kinetics and cell morphologies are available on ModelDB (https://senselab.med.yale.edu/ModelDB/. Accession Numbers: principal relay cell: 279; interneuron: 140249; reticular cell: 17663.)

- **LGN principal relay cell:** Morphology and kinetics of LGN principal relay cell were adapted from [4]. A morphology file of 200 compartments was used (Figure 2, left).
- **Interneuron:** Morphology and kinetics of thalamic interneurons were based on [10] (Figure 2, middle). For a full list of parameters, equations and a detailed description of channel properties and functions, see [10].
- **PGN reticular cell:** Morphology and kinetics of PGN reticular cells were adapted from [3]. Two versions of the model (with 80 or 230 compartments) were tested and gave identical results. Reticular cell morphology of 80 compartments was used in the model (Figure 2, right).
- **Cortical feedback:** Detailed mechanistic models of cortical neurons are not the focus of this project, thus Poisson-driven cortical feedback, instead of biologically detailed cortical neuron models, was used.

2.2.3 Connecting the Neurons. In this study, we constructed NEURON templates for principal relay cells, interneurons and reticular cells based on morphology files. NEURON template is an object

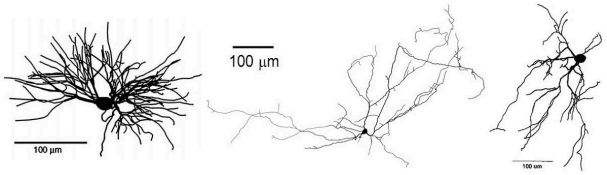

Figure 2: **Morphologies of LGN and PGN cells. Left: LGN principal relay cell. From [4]. Middle: LGN interneuron. From [10]. Right: PGN reticular cell. From [3].**

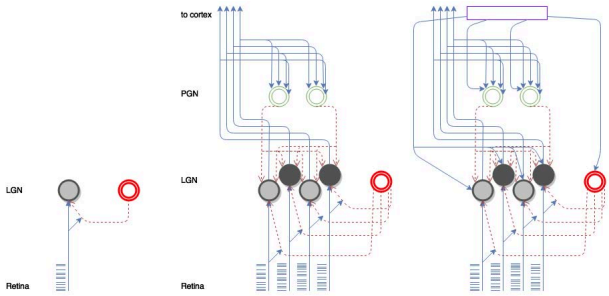

Figure 3: **Topologies of network models in this study. Left: simplest topology which implemented the thalamic triad. Middle: topology of the LGN–PGN loop without modulatory projections from visual cortex. Right: topology of the LGN–PGN–cortex loop. Light gray circle: LGN principal relay cell receiving from ON-center retinal ganglion cell; dark gray circle: LGN principal cell receiving from OFF–center retinal ganglion cell; green circle: PGN reticular cell; red circle: LGN interneuron; solid blue line: excitatory connection; dashed red line: inhibitory connection; blue bar: Virtual-Retina-generated spike train; purple rectangle: cortical feedback. Circles do not represent actual neuronal morphologies implemented in network models.**

definition from which multiple copies of a prototype, such as a cell morphology, can be created [1]. Templates were loaded in the main .hoc file for accessing all the compartments and biophysical settings.

A number of studies have investigated the functional connectivity within the LGN–PGN loop. Parameters that could not be identified with experimental literature or calculation were refined through parameter search [2, 21].

The triadic arrangement of the thalamus is commonly known, but there is not yet a clear explanation of both how the LGN–PGN loop is organized in detail and how the reticular cells in the PGN mutually inhibit one another [23]. Therefore, we fine-tuned the models to achieve a result consistent with experimental findings [7, 16, 24]. Network topologies implemented in this study are shown in Figure 3.

(1) **Topology A:** This topology has one principal relay cell and one interneuron, both receiving inputs from a retinal ganglion cell (Figure 3, left). This model was used to test whether Virtual Retina produces reasonable outputs, and to explain how the thalamic triad deals with incoming inputs at different levels of contrast.
(2) **Topology B:** Topology B [17] was used to examine the perigeniculate contribution to the firing pattern of principal

relay neurons (Figure 3, middle). Relay cell is inhibited by, while sending excitatory projections to, reticular cells. The interneuron forms one triad with each relay cell and one of the retinal terminals.

- Topology B, Version 1: 4 principal relay cells, 1 interneuron, 2 reticular cells and 4 retinal ganglion terminals.
- Topology B, Version 2: 16 principal relay cells, 4 interneurons, 12 reticular cells and 16 retinal ganglion terminals for improved biological plausibility [7, 30].

(3) **Topology C:** Topology C was implemented to assess the effect of cortical modulation on the LGN–PGN loop (Figure 3, right). Approximately 100 Poisson-driven trains were fed into one LGN principal relay cell [27]. Topology C has not been tested against experimental findings due to the greater parameter space.

- Topology C, version 1: 4 principal relay cells, 1 interneuron, 2 reticular cells and 4 retinal ganglion terminals.
- Topology C, version 2: 16 principal relay cells, 4 interneurons, 12 reticular cells and 16 retinal ganglion terminals.

2.3 Visual Stimuli

Drifting sinusoidal gratings [16, 24] and flashing light spots [7] were used to evaluate the model. Images of 6 Hz drifting sinusoidal gratings with 0, 10%, 40% and 100% contrast were processed with the Virtual Retina simulator (Figure 4). Each trial included visual stimulus presentation of 1920 ms, with the first 480 ms removed to avoid initial transients artifacts introduced by Virtual Retina (personal communication from A. Wohrer). 10-20 trials were made for each level of contrast [24].

Flashing light spots of increasing diameter at 40% contrast were used to tune the LGN–PGN model during the setup stage, and later on to verify the effect of stimulus size on firing patterns of both LGN principal relay cells and PGN reticular cells. Flashing spots of 1.5, 2.0, 3.0 and 5.0 deg diameters were used (Figure 5, upper). Each trial lasted 2400 ms, with the first 400 ms removed to allow the network to settle into a stable state (personal communication from A. Wohrer). Recording was done for the following 2000 ms: during the first 400 ms no light spot stimulus was presented (pre-stimulus period), then a light spot was switched on for 800 ms (stimulus On-period) and then switched off for the last 800ms (post-stimulus period) (Figure 5, lower). 100 trials were made for each light spot size [7].

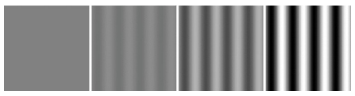

Figure 4: Drifting sinusoidal gratings. Spatial frequency: 0.15 cycles per centimeter; temporal frequency: 6Hz. Levels of contrast from left to right: 0, 10, 40 and 100%.

3 RESULTS

3.1 Topology A

Results obtained from the simplest thalamic triad model were averaged over 10 trials for each contrast level. Saturation effect (a given

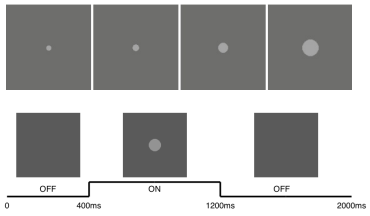

Figure 5: Upper: Flashing light spots of increasing sizes. Level of contrast: 40%. Light spot diameters from left to right: 1.5, 2.0, 3.0 and 5.0 deg. Lower: Example of a 2000 ms trial. Size of the flashing light spot: 5.0 deg.

increment of contrast led to a smaller increment of response in LGN principal cells than in retinal ganglion cells), as in [16], could already be replicated with this simplest topology (Figure 6). However, firing rates from both retinal ganglion cell and LGN principal relay cell were significantly higher than experimental data. Due to the over-activation of Virtual Retina artificial retinal ganglion cells when contrast was 0, change of the saturation curve slope could not be fully replicated in our simulations.

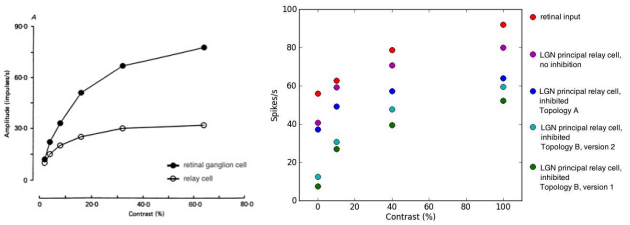

Figure 6: Contrast saturation curves. Left: results from [16]. Upper curve shows data from retinal ganglion cell and lower curve shows data from LGN principal relay cell. B: Results from the simplest triad model and the LGN–PGN model. Red: response from retinal ganglion cell (generated by Virtual Retina); magenta: response from LGN principal relay cell, not inhibited; blue: response from LGN principal relay cell in the simplest triad model, inhibited by interneuron; green: response from an ON-center LGN principal relay cell in Topology B, version 1; cyan: response from an ON-center LGN principal relay cell in Topology B, version 2. Response amplitudes were averaged over 10-20 trials.

3.2 Topology B

In [7], no detectable responses were recorded from the PGN reticular cell when the flashing light spot was set to 1.5 deg (Figure 7). However, in the model with one PGN reticular cell and one LGN principal relay cell, transient responses were evoked when the size of the light spot was 1.5 deg. Therefore, network topology consisting of one LGN neuron and one PGN neuron yielded poor consistency with experimental observations on PGN reticular cell activity patterns. More PGN reticular cells were added into the model to improve its biological plausibility.

3.2.1 Topology B, Version 1. LGN principal relay cell model replicated the progressively decreasing activity of biological principal relay cells, when presented with stimuli of increasing sizes. However, the rebound response of burst discharges when the light spot was set to a size of 5.0 deg was not seen (Figure 8, blue traces). Response amplitudes were significantly higher than reported in [7] after the stimulus onset and throughout the whole stimulus

On-period. Possible explanations include: (a). the LGN interneuron could not sufficiently inhibit LGN principal cells, or (b). principal relay cell was intrinsically too excitable during the stimulus On-period.

In agreement with experiment, the PGN reticular cell model was not activated by the light spot of size 1.5 deg, as there was no transient response at either stimulus onset or offset. Transient responses were observed at both stimulus onset and offset when the size of the light spot increased to 2.0 deg. At 3.0 deg, there was a visible increase in response amplitude at stimulus onset and offset. At 5.0 deg, however, the simulation result was no longer consistent with experimental observations: response amplitudes at both stimulus onset and offset decreased, although only slightly.

Another inconsistency was observed during the stimulus On-period. In experimental recordings, response amplitudes in PGN cells during the stimulus On-period were always similar to, or lower than, spontaneous activity. This was not observed in any of the simulations. This may be caused by the strong activity of LGN principal relay cells during the stimulus On-period. In addition, when the light spot size was 2.0 deg, the response amplitude at stimulus onset was too strong.

3.2.2 Topology B, Version 2. Results from Topology B, version 2 yield considerable similarities with Topology B, version 1 (Figure 8, red traces). The LGN principal relay cells emitted the strongest response at stimulus onset when a light spot of size 1.5 deg was presented. As the spot size increased, the amplitude of the transient response at stimulus onset was reduced. No transient response was evoked in PGN reticular cells when light spot size was 1.5 deg. As the size increased, transient activity was observed, with progressively increasing amplitude.

However, LGN and PGN cells in Topology B, version 2 produced different activity patterns under certain experimental conditions. For example, the amplitude of the transient response at stimulus onset in the second condition was not abnormally high as observed in Topology B, version 1. Furthermore, a visible increase in activity was found when light spot size increased from 3.0 deg to 5.0 deg, which led to an improved consistency with the experimental observations. However, under a light spot stimulus of 5.0 deg, the firing rate of LGN principal relay cells in Topology B, version 2 was significantly higher during the stimulus On-period than in Topology B, version 1.

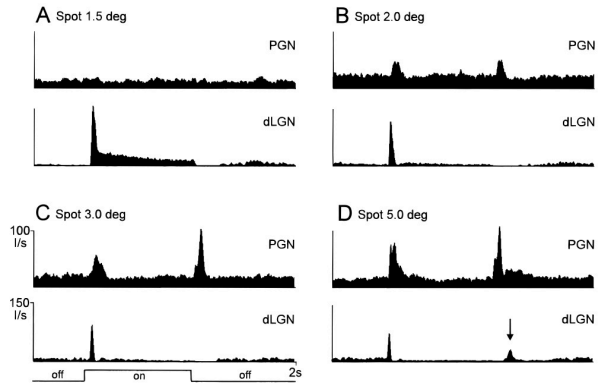

Figure 7: Experimental results from [7]. Peri-stimulus time histogram (PSTH) showing activity patterns of PGN reticular cell (upper histogram) and LGN X-ON principal relay cell (lower histogram) under flashing light spots of different sizes. Result in each histogram was averaged over 100 trials.

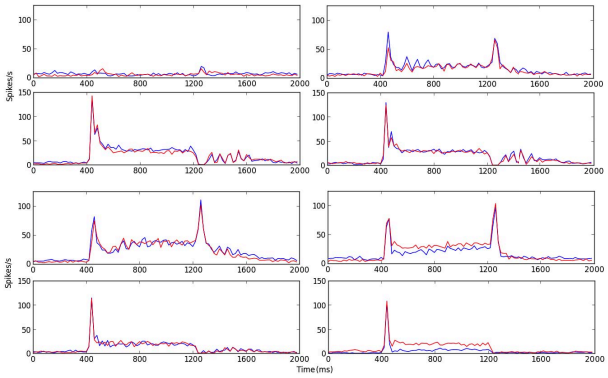

Figure 8: Results from the LGN–PGN model, without cortical modulation. Histograms presented in the same order as in Figure 7. Blue trace: result from Topology B, version 1; red trace: result from Topology B, version 2. Result in each histogram was averaged over 100 trials, bin-size = 20 ms.

4 DISCUSSION

Neuroscience has been an inspiration for the deep learning community at many scales. At the system and pathway scale, researchers were able to create a highly abstracted version of the biological visual processing streams, which later gave rise to convolutional neural networks (CNN), a representation of the visual processing hierarchy that is becoming a practical solution to face recognition, image classification, car detection in autonomous driving and speech processing. More recently, with the aim of understanding how the credit assignment problem could be solved by biological brain circuitry, studies have returned to the scale of single neurons and looked into the role of multi-compartmental neurons in biologically-plausible deep learning [8].

Neurons in the ANNs are known to be fundamental units that store weights. However, in the more biologically plausible multi-compartmental neurons, the story gets complicated due to their innate electrotonic structures [20]. Therefore, an abstracted implementation of biological neurons in deep learning models may help us find alternative network connectivities that localize the global computation load.

Neocortical information processing and pyramidal neuron morphologies have led to significant improvements on deep neural networks [8, 11]. In the meantime, properties of subcortical neurons and their implications for deep learning remain less explored. Results from the present study revealed localized information processing and compression in the thalamus, indicating a biological structure that could be adapted and realized for novel deep learning frameworks.

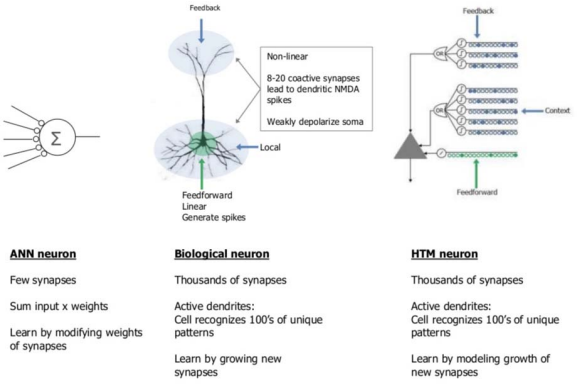

Figure 9: Real-time streaming data analysis with HTM (Hierarchical Temporal Memory) neurons [11], an example of how the neuron is either represented over-simplistically or in the form of HTM neurons. While it is known that our biological system can conduct highly complicated tasks at ease, scene segmentation and other visual tasks that involve rotation and motion are particularly challenging for deep neural networks (DNN). Source: Numenta.

4.1 Visual Processing and Computational Modeling

In the *in vivo* experiment conducted by Hubel and Wiesel [15], they discovered that the neurons fire when mammals were presented with vertical, horizontal or diagonal bars. They have also demonstrated neurons were organized in a columnar architecture to facilitate visual perception. This task-oriented representation in which the biological neuronal cells (simple, complex or hypercomplex) in the visual cortex look for specific characteristics has since become the *de facto* method to construct *in silico* representation in computer vision, more specifically, in CNNs.

While biologists, computational neuroscientists and machine learning researchers have conducted numerous studies *in vivo, in vitro* and *in silico*, there still seems to be either simplistic or overcomplicated explanations of how artificial neural networks (ANN) imitate the biological neurons (Figure 9). Although biophysics, neuroscience, neurophysiology and computational biology have been long lived in isolation, recent findings have fortunately led to novel experimental interpretation of the physiological data as well as computational methods such as Capsule Networks.

4.2 The Biophysics behind Cortical Hierarchies and Deep Learning

Initially introduced by Marr in 1982 [18], ensemble deep cortical hierarchies are well understood today in both neuroscience and computation vision. Parallel retino-geniculo-cortical pathways (parvo- and magno-cellular) are most commonly studied in mammals: Magnocellular (M) pathway is faster, covering coarser spatial inputs involved in motion and space processing while a much slower Parvocellular (P) pathway conveys spatial information of higher resolution. Computationally, researchers have used a linear systems approach to model low-level visual processing. For instance, CNN can demonstrate how neurons in the primary visual cortex eventually paving ways to a retinotopic map of much higher resolution.

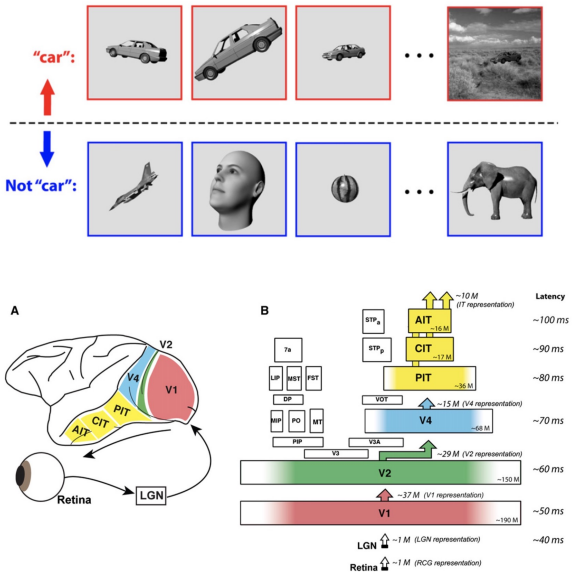

Figure 10: Top: Rapid object recognition (i.e., <200 ms viewing duration) in primates, even under identity-preserving transformations of objects, such as rotation, tilt, position and size change. Bottom: (A): Ventral stream of a macaque monkey brain. (B): Brain regions plotted proportional to the size of its cortical surface area [6] and represented with the approximate total number of neurons shown in millions (M). Adapted from [5].

Beside the observable structural differences, there seems to be reasonable general agreement between the anatomical hierarchies of magno-, parvo- and konio-cellular pathways in humans and non-humans. Mammalian brain solves visual representation rapidly via its ventral and dorsal pathways (Figure 10). In the meantime, there is increasing evidence that even avians and amphibians have visual systems which are far more sophisticated than what we have come to believe: a cascade of reflexive, largely forward propagated computation [5] as compared to the differential programmed back-propagation in deep learning. It is possible today to pick neurons and dissect their circuitry at the synaptic level by combining results from functional and structural studies. Ongoing projects from initiatives such as Human Brain Project, Google Brain, Baidu Brain, BRAIN have given rise to promising research outcomes.

5 CONCLUSION AND FUTURE WORK

Despite considerable success of deep learning models, progress has only been made on basic human perception tasks such as object recognition. Meanwhile, we are struggling to understand how cortical circuitry give rise to certain behavior. To achieve a considerable level of understanding, we need more mathematical, theoretical and biological knowledge. Therefore, sufficient data-driven evidence of thalamocortical connectivity is needed to conclusively understand sensory information processing, and further, to potentially make approximations to biologically-realistic decision making.

Thus, the next step is to delve deeper into the circuitry of the (mammalian) brain. This will involve the following: (a) fine-tuning parameters of the LGN model and its associated neurotransmission, (b) investigating the retinotopic mappings and receptor properties

of the LGN and (c) understanding the functional implications of the two response modes of principal relay cells in the LGN: tonic and burst.

An integration of deep learning and neuroscience could lead to optimized research effort in both areas. Capsule networks [22], along with recently released models inspired by neocortical communication via the thalamus (ThalNet) [9] and multi-compartmental neocortical pyramidal neurons [8], will help us to create better toolboxes for developing real-world applications. In future work, we will implement a biologically-plausible connectivity model of the thalamocortical circuitry as we continue our research in Capsule Networks. Results from the ongoing studies will be presented in the form of conference papers, talks and lectures.

REFERENCES

[1] N. T. Carnevale and M. L. Hines. 2006. *The NEURON book*. Cambridge University Press.

[2] A. Destexhe, D. Contreras, and M. Steriade. 1998. Mechanisms underlying the synchronizing action of corticothalamic feedback through inhibition of thalamic relay cells. *Journal of neurophysiology* 79, 2 (1998), 999–1016.

[3] A. Destexhe, D. Contreras, M. Steriade, T. J. Sejnowski, and J. R. Huguenard. 1996. In vivo, in vitro, and computational analysis of dendritic calcium currents in thalamic reticular neurons. *Journal of Neuroscience* 16, 1 (1996), 169–185.

[4] A. Destexhe, M. Neubig, D. Ulrich, and J. Huguenard. 1998. Dendritic low-threshold calcium currents in thalamic relay cells. *Journal of Neuroscience* 18, 10 (1998), 3574–3588.

[5] J. J. DiCarlo, D. Zoccolan, and N. C. Rust. 2012. How does the brain solve visual object recognition? *Neuron* 73, 3 (2012), 415–434.

[6] D. J Felleman and D. C. Van Essen. 1991. Distributed hierarchical processing in the primate cerebral cortex. *Cerebral cortex (New York, NY: 1991)* 1, 1 (1991), 1–47.

[7] K. Funke and U. T. Eysel. 1998. Inverse correlation of firing patterns of single topographically matched perigeniculate neurons and cat dorsal lateral geniculate relay cells. *Visual neuroscience* 15, 4 (1998), 711–729.

[8] J. Guerguiev, T. P. Lillicrap, and B. A. Richards. 2017. Towards deep learning with segregated dendrites. *eLife* 6 (2017).

[9] D. Hafner, A. Irpan, J. Davidson, and N. Heess. [n. d.]. Learning Hierarchical Information Flow with Recurrent Neural Modules. In *Advances in Neural Information Processing Systems*. 6727–6736.

[10] G. Halnes, S. Augustinaite, P. Heggelund, G. T. Einevoll, and M. Migliore. 2011. A multi-compartment model for interneurons in the dorsal lateral geniculate nucleus. *BMC neuroscience* 12, 1 (2011), P222.

[11] J. Hawkins, S. Ahmad, and Y. Cui. 2017. A Theory of How Columns in the Neocortex Enable Learning the Structure of the World. *Frontiers in neural circuits* 11 (2017), 81.

[12] M. L. Hines and N. T. Carnevale. 1997. The NEURON simulation environment. *Neural computation* 9, 6 (1997), 1179–1209.

[13] M. L. Hines, A. P. Davison, and E. Muller. 2009. NEURON and Python. *Frontiers in neuroinformatics* 3 (2009), 1.

[14] A. L. Hodgkin and A. F. Huxley. 1952. A quantitative description of membrane current and its application to conduction and excitation in nerve. *The Journal of physiology* 117, 4 (1952), 500–544.

[15] D. H. Hubel and T. N. Wiesel. 1962. Receptive fields, binocular interaction and functional architecture in the cat's visual cortex. *The Journal of physiology* 160, 1 (1962), 106–154.

[16] E. Kaplan, K. Purpura, and R. M. Shapley. 1987. Contrast affects the transmission of visual information through the mammalian lateral geniculate nucleus. *The Journal of physiology* 391, 1 (1987), 267–288.

[17] Y-W. Lam and S. M. Sherman. 2005. Mapping by laser photostimulation of connections between the thalamic reticular and ventral posterior lateral nuclei in the rat. *Journal of Neurophysiology* 94, 4 (2005), 2472–2483.

[18] D. Marr. 1982. Vision: A computational approach. (1982).

[19] D. A. McCormick and T. Bal. 1997. Sleep and arousal: thalamocortical mechanisms. *Annual review of neuroscience* 20, 1 (1997), 185–215.

[20] T. M. McKenna, J. L. Davis, and S. F. Zornetzer. 2014. *Single neuron computation*. Academic Press.

[21] J. Rogala, W. J. Waleszczyk, S. Łęski, A. Wróbel, and D. K. Wójcik. 2013. Reciprocal inhibition and slow calcium decay in perigeniculate interneurons explain changes of spontaneous firing of thalamic cells caused by cortical inactivation. *Journal of computational neuroscience* 34, 3 (2013), 461–476.

[22] S. Sabour, N. Frosst, and G. E. Hinton. [n. d.]. Dynamic routing between capsules. In *Advances in Neural Information Processing Systems*. 3859–3869.

[23] M. V. Sanchez-Vives, T. Bal, and D. A. McCormick. 1997. Inhibitory interactions between perigeniculate GABAergic neurons. *Journal of Neuroscience* 17, 22 (1997), 8894–8908.

[24] G. Sclar. 1987. Expression of "retinal" contrast gain control by neurons of the cat's lateral geniculate nucleus. *Experimental Brain Research* 66, 3 (1987), 589–596.

[25] S. M. Sherman. 2004. Interneurons and triadic circuitry of the thalamus. *Trends in neurosciences* 27, 11 (2004), 670–675.

[26] S. M. Sherman and R. W. Guillery. 2001. *Exploring the thalamus*. Elsevier.

[27] S. M. Sherman and C. Koch. 1986. The control of retinogeniculate transmission in the mammalian lateral geniculate nucleus. *Experimental Brain Research* 63, 1 (1986), 1–20.

[28] A. M. Sillito and H. E. Jones. 2002. Corticothalamic interactions in the transfer of visual information. *Philosophical Transactions of the Royal Society B: Biological Sciences* 357, 1428 (2002), 1739–1752.

[29] M. Steriade, L. Domich, G. Oakson, and M. Deschenes. 1987. The deafferented reticular thalamic nucleus generates spindle rhythmicity. *Journal of neurophysiology* 57, 1 (1987), 260–273.

[30] W. J Waleszczyk, M. Bekisz, and A. Wróbel. 2005. Cortical modulation of neuronal activity in the cat's lateral geniculate and perigeniculate nuclei. *Experimental neurology* 196, 1 (2005), 54–72.

[31] A. Wohrer and P. Kornprobst. 2009. Virtual retina: a biological retina model and simulator, with contrast gain control. *Journal of computational neuroscience* 26, 2 (2009), 219–249.